Breast Cancer Genetic Mutation Classification - Report

By Deva Dharshini Ravichandran Lalitha

1. Introduction

This project aims to enhance the classification of breast cancer genetic mutations using 3D MRI data—a domain with limited prior research and few publicly available datasets. The complex nature of MRI signals and the typically small sample sizes make this a challenging task. More importantly, it is not possible to directly identify genetic mutations such as BRCA1/2 solely from breast MRI; such mutations must be confirmed through genetic testing. Traditional methods often rely on handcrafted features or transfer learning from non-medical or 2D modalities, which may not generalize well to 3D medical imaging [1], [2]. In this study, mutation labels are derived from confirmed genetic testing results. To address existing gaps in the literature, we evaluate multiple 3D convolutional neural networks (CNNs) and preprocessing pipelines, leveraging recent advancements in medical vision models and data augmentation techniques to improve classification accuracy.

2. Dataset and Preprocessing

2.1. Dataset Distribution

The de-identified dataset has a total of 847 volumes with class labels - mutation or no mutation. The dataset was split into training, validation and test sets with 60-20-20 ratio. The distribution of the data after splitting is presented in table 1.1.

The dataset also had the respective metadata such as orientation, pixel spacing and study descriptions which were later used for filtering and preprocessing. Figure 1.1 represents the distribution of different studies (“MR BREAST BILATERAL”, “MR BREAST BIOPSY”, etc.,). Studies with study descriptions “MR BREAST BILATERAL” were retained, “non-BILATERAL” or “Biopsy” studies were excluded.

	No Mutation	**Mutation**
Train	259	333
Test	50	78
Validation	58	69
Total	367	480

Table 1.1 : Train, Validation and Test Data Distribution

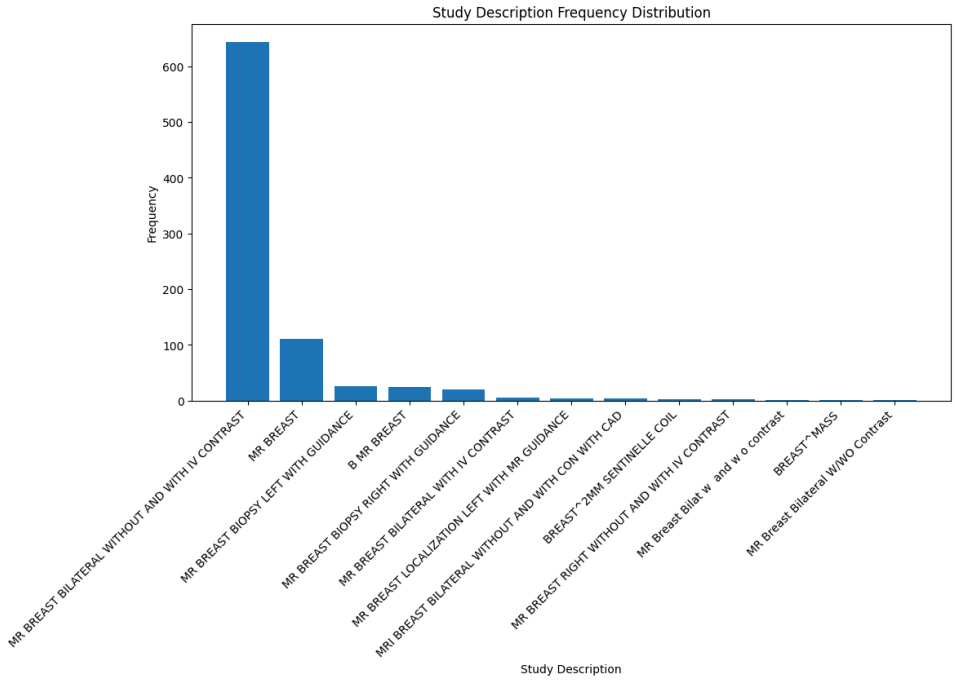

Figure 1.1 : Distribution of different Study Description

2.2. Bit-Depth Reduction

To ensure consistent input across all MRI scans, different image data types were standardized:

2.2.1. **Normalization**: 16-bit volumes were min-max normalized and were converted to the range [0,255], Whereas the first channel was chosen and normalized to the same range for 8-bit RGBA volumes

2.2.2. **Bit-Depth Conversion**: After normalization, the floating-point image was cast to uint8, reducing storage and computation while preserving the relative contrast.

2.3. Resampling

Resampling is the process of interpolating voxel intensities to achieve a uniform spatial resolution across all three dimensions of a 3D image. MRI volumes had different pixel spacing and slice thickness. The distribution of the pixel spacing and slice thickness is presented in figure 1.2 below. All MRI volumes were resampled to a near-isotropic

spacing of 1.1 × 1.1 × 3.0 mm using B-spline interpolation to standardize voxel dimensions across scans.

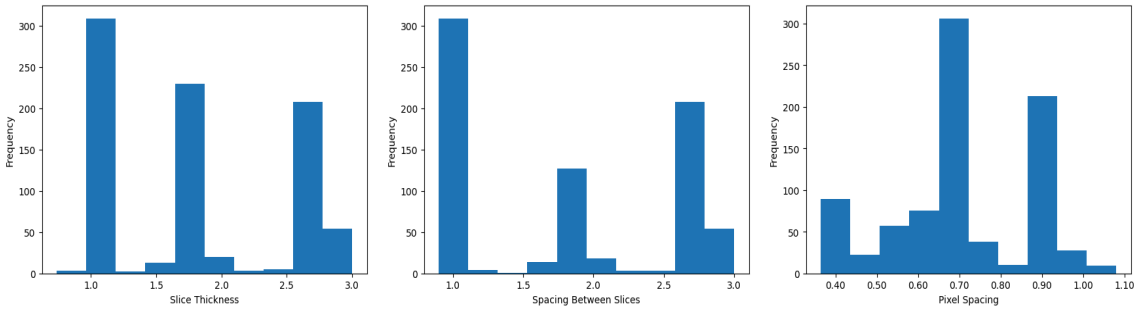

Figure 1.2: Distribution of Slice Thickness, Spacing between slices and Pixel Spacing of the MRI volumes

2.4. Histogram Equalization

Histogram equalization is a contrast enhancement technique that redistributes pixel intensities to achieve a more uniform histogram, improving the visibility of structures in an image. This technique helped in improving the contrast of the MRI volumes. Slices from the MRI volumes before and after histogram equalization and their corresponding histogram are presented in the figure 1.3.

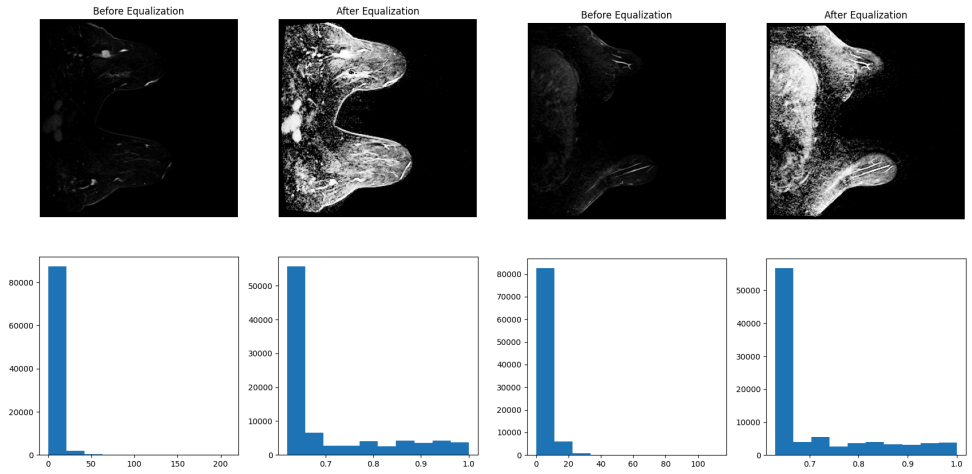

Figure 1.3: Before and After Histogram Equalization

2.5. Background Removal

To ensure that only anatomically relevant foreground structures are retained for downstream model connected component analysis was applied to binarized MRI volumes to identify and isolate the largest contiguous region of interest—typically corresponding to breast tissue—while removing small disconnected components (e.g.,

background noise or scanner artifacts). The result of background removal is demonstrated in the figure below

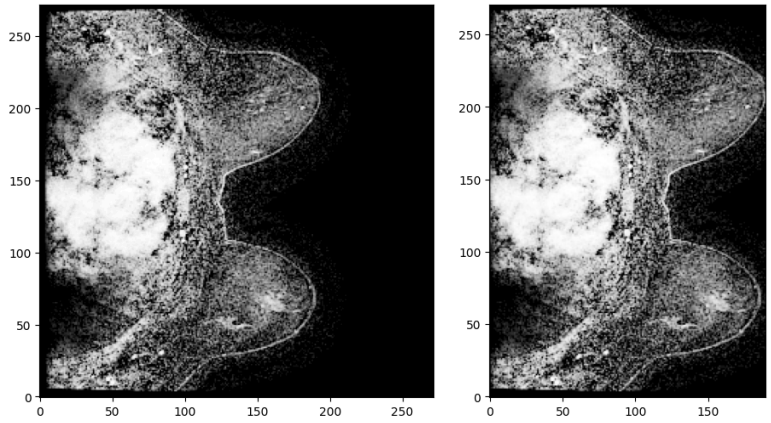

Figure 1.4: Background Removal - Before and After

2.6. Orientation Handling

The dataset exhibited a varied distribution of DICOM orientations due to differences in scanner protocols and acquisition settings. The distribution of the image orientation is presented in the below table. However, after conversion to NIfTI format, all volumes were consistently reoriented to **LAS (Left-Anterior-Superior)**.

In the LAS orientation: **L (Left)** → Rows increase from **left to right**, corresponding to a row direction vector of *(1, 0, 0)*. **A (Anterior)** → Columns increase from **posterior to anterior**, corresponding to a column direction vector of *(0, 1, 0)*. **S (Superior)** → Slices are stacked from **inferior to superior**, along the Z-axis *(0, 0, 1)*.

This uniform orientation ensures consistent anatomical alignment across all subjects, which is essential for consistent 3D convolution, data augmentation, and interpretation of spatial features during model training.

Image Orientation	View
('-0.0', '1.0', '0.0', '-0.0', '-0.0', '-1.0')	Sagittal
('1.0', '4.897e-12', '0.0', '-4.897e-12', '1.0', '0.0')	Axial
('-1.0', '-0.0', '0.0', '-0.0', '-1.0', '0.0')	Axial
('1.0', '0.0', '0.0', '0.0', '1.0', '0.0')	Axial
('1.0', '-2.05103e-10', '0.0', '2.05103e-10', '1.0', '0.0')	Axial

Table 1.2: Orientation values from Meta-data and respective views

3. Methods

We explored two approaches to address the problem at hand: (1) linear probing the image encoder of a medical foundation model (M3D), and (2) training domain-specific image encoders using various transfer learning strategies.

3.1. Linear Probing using M3D Embeddings

M3D is a large-scale 3D multi-modal medical foundation model trained on M3D-Data, which includes 120K image–text pairs and 662K instruction–response pairs curated for diverse 3D medical tasks [1]. We extracted 768-dimensional embeddings from the pretrained M3D model (trained on CT scans) and passed them to a Multi-Layer Perceptron (MLP) for mutation classification

3.2. Residual Networks 3D (ResNet10, ResNet18, ResNet50)

We also trained 3D Residual Networks (ResNet10, ResNet18, ResNet50) directly on the MRI volumes for mutation classification. To evaluate the impact of transfer learning, we experimented with the following weight initialization and transfer learning strategies - **Random initialization, Kinetics pretrained weights** (trained on action recognition tasks), **MedicalNet pretrained weights** (trained on a large corpus of 3D medical images)

4. Experiments and Results

4.1. Optimization Strategies

The model training process employed several optimization strategies to ensure stable convergence and improved generalization. Binary Cross-Entropy with Logits was used as the loss function, suitable for binary classification tasks. The Adam optimizer with a learning rate of 1e-3 was selected for its adaptive learning capabilities. To further refine learning, three different learning rate schedulers were experimented with: ReduceLROnPlateau, CyclicLR, and MultiStepLR. Early stopping was also implemented with a patience of 15 epochs to prevent overfitting by halting training once the validation performance plateaued. ROC curves were used to select optimal classification thresholds for each model individually using geometric means

4.2. Evaluation Metrics

Model performance was evaluated using key classification metrics—Precision, Recall, and Area Under the Receiver Operating Characteristic Curve (AUC)—to

provide a comprehensive assessment of each model's effectiveness. The results are presented in table 1.9. Resnet-50 initialized with pre-trained weights from Kinetics seems to perform the best in terms of precision and accuracy, whereas ResNet-18 trained with random weight initialization provides the best recall. It is also interesting to note that linear probing with M3D seems to provide comparable results even though the foundation model was trained on CT and not MRI

4.3. Interpretability

To enhance interpretability and model explainability, UMAP was employed to visualize the M3D embeddings, while Grad-CAM++ was used to generate activation maps. Figures 1.5 and 1.6 present the Grad-CAM++ maps for true positives and false positives, respectively, of the best-performing model. For true positives, the model predominantly focuses on the breast region. However, in some cases, it also appears to attend to the cardiac muscle.

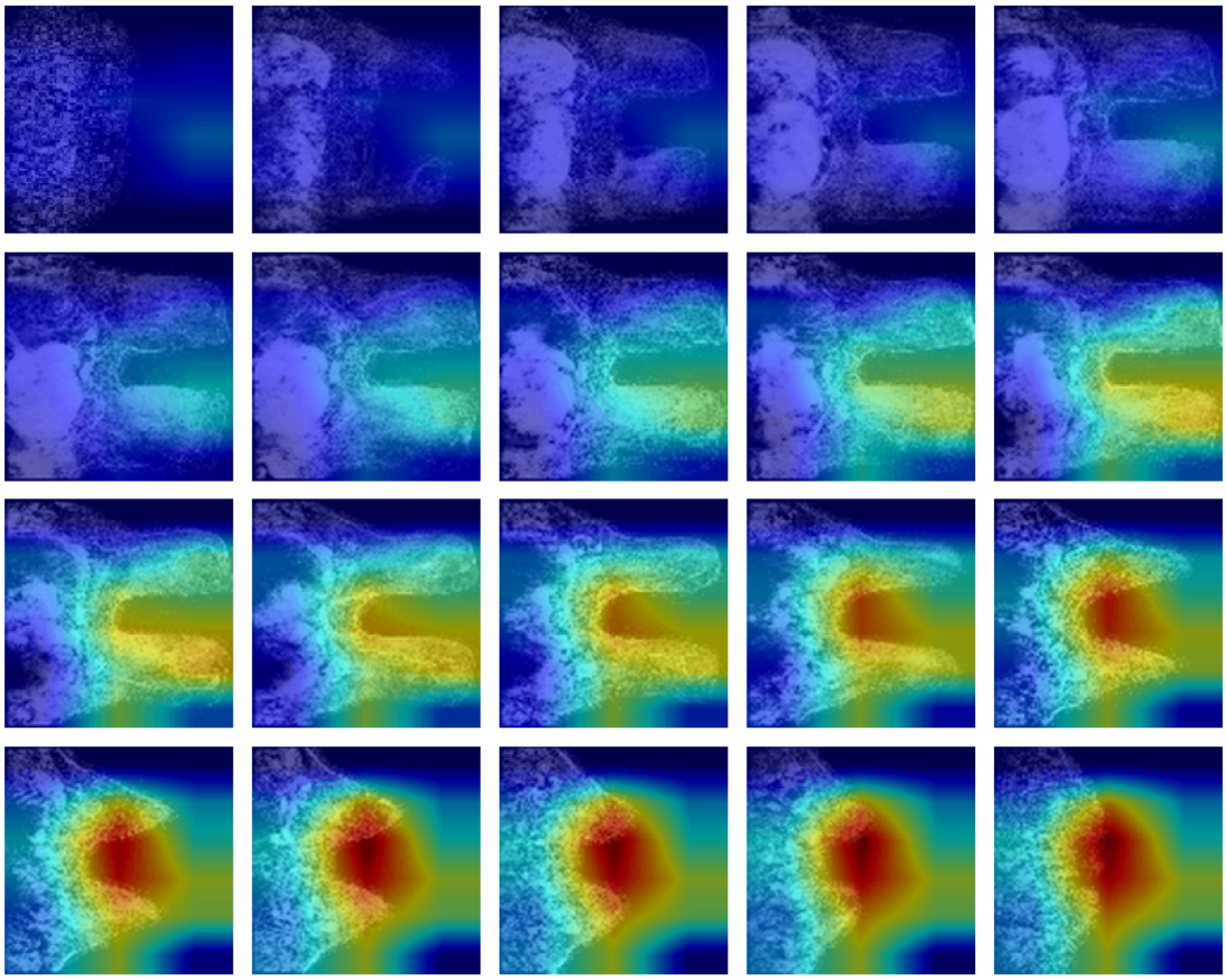

Figure 1.5: Grad-cam of true positive case (Predicted probability - 0.99)

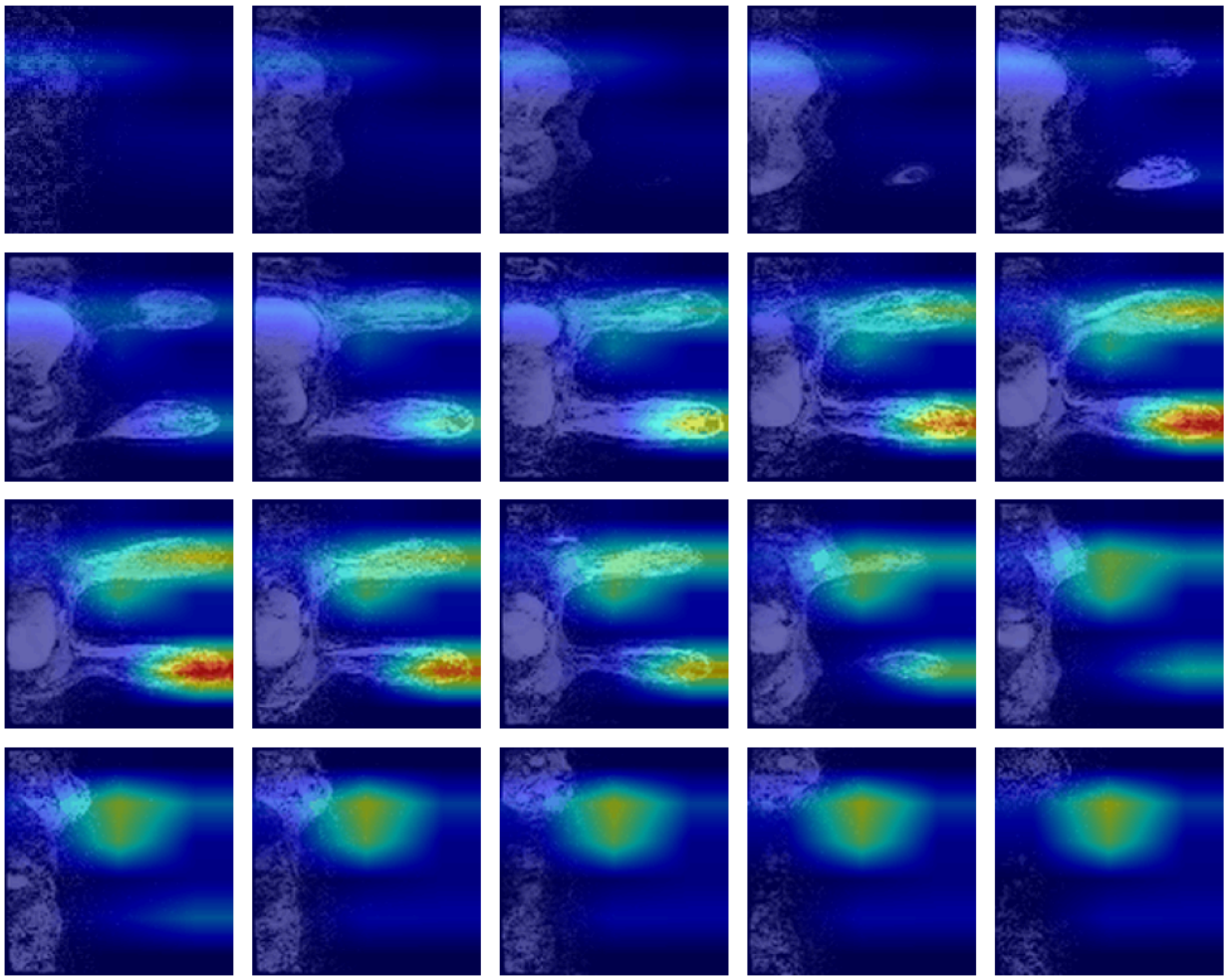

Figure 1.6: Grad-cam of false positive case (Predicted probability - 0.75)

	Weights	Precision	Recall	AUC
Resnet10	Random	0.8889	0.8312	0.8356
	MedicalNet	0.8873	0.8182	0.8291
Resnet18	Random	0.8571	**0.8571**	0.8186
	Kinetics	0.8923	0.7532	0.8066
	MedicalNet	0.9355	0.7532	0.8366
Resnet50	Random	0.9000	0.8182	0.8391
	Kinetics	**1.0000**	0.6883	**0.8442**
	MedicalNet	0.9455	0.6753	0.8077
Linear Probing	M3D	0.7590	0.8181	0.8223

Table 1.3: Precision, Recall, AUC Result comparing different versions and pre-training weights

5. Future Work and Next Steps

Future work will focus on several key areas to enhance the robustness and generalizability of the model. External validation will be conducted using publicly available datasets to assess performance across different cohorts. Interpretability will be further extended by applying Grad-CAM++ visualizations to all pretrained models, offering deeper insights into model decision-making. Additionally, comprehensive hyperparameter tuning and regularization experiments will be performed to optimize model performance. The final phase will involve preparing the best-performing model for deployment, including export and integration into clinical or research pipelines.

6. Conclusion

This study demonstrates the feasibility and effectiveness of using deep learning for breast cancer genetic mutation classification from 3D MRI data. Early experiments with M3D embeddings showed that large-scale pretraining on medical datasets can extract meaningful features even across imaging modalities. Residual 3D networks (ResNet10/18/50) with random weight initializations served as strong baselines, and performance improved with the use of pretrained weights from MedicalNet and Kinetics

datasets. Preprocessing techniques—such as B-spline resampling, histogram equalization, and background removal—played a critical role in standardizing data and enhancing model performance.

Grad-CAM++ visualizations further supported model interpretability by highlighting relevant anatomical regions. While promising results were achieved, especially with MedicalNet-pretrained ResNet models, further improvements are possible through extended hyperparameter tuning, external validation, and model regularization. This work lays a foundation for future efforts in MRI-based genetic mutation prediction and highlights the importance of combining robust preprocessing with domain-adapted models in medical AI research.

7. References

[1] F. Bai, Y. Du, T. Huang, M. Q.-H. Meng, and B. Zhao, “M3D: Advancing 3D Medical Image Analysis with Multi-Modal Large Language Models,” *arXiv preprint arXiv:2404.00578*, Mar. 2024. Available: https://arxiv.org/abs/2404.00578(arXiv)

[2] K. Hara, “3D-ResNets-PyTorch,” GitHub repository, 2018. Available: https://github.com/kenshohara/3D-ResNets-PyTorch

[3] Z. Chen, L. Ma, W. Zhang, et al., *MedicalNet: Pretrained 3D Medical Models for Transfer Learning*, GitHub repository, 2019. [Online]. Available: https://github.com/Tencent/MedicalNet

[4] J. Gildenblat and contributors, “PyTorch library for CAM methods,” GitHub repository, 2021. Available: https://github.com/jacobgil/pytorch-grad-camNature+3arXiv+3GitHub+3